SRTTU

JCARME
ISSN: 2228-7922
Journal of Computational and Applied Research in Mechanical Engineering
Vol. x, No. x, xxxx
jcarme.sru.ac.ir

A Method for Detecting Bubbles in Two-phase Gas-Liquid Flow

P. Hanafizadeh[a,*], A. Sattari[a], S. E. Hosseinidoost[a], M. Molaei[a], and M. Ashjaee[a]

[a] *Center of Excellence in Design and Optimization of Energy Systems, School of Mechanical Engineering, College of Engineering, University of Tehran, Tehran, Iran, P. O. Box: 11155-4563*

Article info:

Received: 00/00/2000
Accepted: 00/00/2018
Online: 00/00/2018

Keywords:
JCARME,
Frequency,
Electronic device,
Image processing,
Numerical,
Theoretical.

Abstract

Detecting bubble in two-phase flow has been a basic issue in two-phase flow systems. A new method for measuring the frequency of bubble formation is presented in this paper. For this purpose, an electronic device was designed and constructed which works based on a change in intensity of laser beam. For this purpose, continues light beam is embedded just above the needle, which is received by a phototransistor. When bubbles go through this light beam, make a deviation on that and change the intensity of light. So, the electrical resistance between two bases of phototransistor changes and this variation sensed by an electronic board. According to the number of interruption and duration time, the frequency of bubble formation can be calculated. Liquid and gas phases of present work are water and air respectively. Tests are performed in constant liquid height (60 mm above the needle), constant needle diameter (1.6 mm), and gas flow rates between 50 to 1200 ml/hr. Also, three other methods utilized for measuring bubble frequency: image processing (IP), numerical modeling, and theoretical model. Results show that with increasing flow rate of the gas phase frequency of formation increases approximately in a linear manner. Validation of methods with IP method shows that the new device has very good accuracy for measuring bubble formation frequency. So because of the simplicity of using and low cost, it can be a superseded method of image processing.

Nomenclature

a	Acceleration
A	Projection area of the bubble
D	Diameter of the bubble
f	Frequency of bubble formation
F_B	Buoyancy force
F_D	Drag force
F_V	Virtual mass force
F_σ	Surface tension force
G	Gravity force
m	Bubble mass
$\dot{m}$	Mass transfer
P	Circumference of the needle
Q	Volumetric flow rate
Re	Reynolds number
u	Velocity
U_f	Volume flux through the face
V	Volume of the bubble
V_C	Volume of the cell

Greek symbols

α_q	Volume fraction
θ	Contact angle of the bubble

*Corresponding author
Email address: hanafizadeh@ut.ac.ir

ρ	Density
σ	Interfacial tension
Subscripts	
g	Gas phase
l	Liquid phase
p	Phase p
q	Phase q

1. Introduction

The dynamic of bubble formation has a major role in diverse applications related to scattering of gas bubbles in liquids such as water treatment, chemical reactors, metallurgy, and medical. Also, it is an important subject in the context of two-phase heat transfer [1–3]. This phenomenon is affected by different parameters such as the equivalent diameter of injection, the geometry of injection, gas flow rate, liquid and gas physical properties, the height of the liquid column, and wettability.

On the terrain of bubble formation in various conditions, abundant works have been done. For instance, Davidson and Amick [4] worked on formation of gas bubbles at horizontal orifices. Influence of different parameters was examined on the formation of bubble such as the diameter of the orifice, the volume of the chamber, and physical properties. In another research, Ramakrishnan, et al. [5] studied on bubble formation under constant flow conditions. In this paper a model based on two-step mechanism of bubble formation is proposed. Also, Akita and Yoshida [6] investigated bubble size, interfacial area, and liquid-phase mass transfer coefficient in bubble columns. They presented dimensionless correlations for the average bubble size. In another paper, Sada et al. [7] done a research on bubble formation in flowing liquid. They found that the bubble size in flowing liquid decreases with increasing superficial liquid velocity and with decreasing gas flow rate. Furthermore, Tsuge and Hibino [8] investigated bubble formation from an orifice submerged in liquids. The effects of various factors, such as orifice diameter, gas physical properties and gas chamber on the bubbles volume were explored in this paper. Also, Kim et al. [9] developed a theoretical model for bubble and drop formation in flowing liquids in microgravity by using a force balance. They found that the bubbles are detached from the nozzle only by the liquid flow drag. Byakova et al. [10] examined influence of wetting conditions on bubble formation at orifice in an inviscid liquid mechanism of bubble evolution. They concluded that the influence of operating variables on formation of bubble is different under various wetting conditions. Corchero et al. [11] done experimental investigations on effects of wetting conditions and flow rate on bubble formation at orifices. Also, a simple model of the bubble shape at detachment was proposed that gives results in good agreement with experiments at small flow rates. Qu and Qiu [12] worked on bubble dynamics under a horizontal microheater array. They studied effects of Marangoni, buoyancy, and drag forces on the bubble dynamic phenomena have been utilizing experimental data. In another work, Ohta et al. [13], done a computational study of dynamic motion of a bubble rising in Carreau model fluids. They utilized VOF numerical model in order to simulating mechanism of bubble formation. They discussed bubble rise motion in shear-thinning fluids in terms of the effective viscosity, the effective Reynolds number, and the effective Morton number. In another work, Vafaei et al. [14] investigated bubble growth rate from needle nozzles. They realized that the bubble volume expansion rate follows a cyclic behavior for the substrate nozzles while it shows a smooth decrease after an initial increase for the needle nozzles. Finally, Di Bari and Robinson [15] done an experimental study of gas injected bubble growth from submerged orifices. The quasi-static growth and departure characteristics showed little dependence on the growth rate while have a notable dependence on the orifice size.

Among the parameters influencing the formation of bubbles, frequency of bubble formation and its relationship with gas flow rate are major issues for bubble formation, which have been attracted many attentions in the literature. Almost in all researches it is found that bubble frequency increases with increasing of gas flow rate [16–20]. Most researchers utilized a high speed camera and image processing method to computing frequency of bubble formation which

has high cost and time consuming. Also, in industrial applications of bubble formation, image processing can't be used because of need to momentary measuring frequency. Some researchers measured frequency by counting number of bubbles generated in a specified interval that is not an accurate method nowise. Another method for measuring bubble formation frequency that has been utilized in some researches is using different kind of probes like optical and conductivity probes which are high costs as high speed cameras. For instance, Harvey et al. [21] measured vapor bubble using image analysis. They presented a method of computer image analysis which determines flow quantities of a single vapor bubble as it evolves near a rigid boundary. Also, Davidson et al. [22] measured the frequency of bubble formation by stroboscopic illumination. By experimental investigations, they concluded that frequency of bubble formation decreases by increasing of orifice diameter. In another paper, Lguchi et al. [23] investigated effects of cross-flow on the frequency of bubble formation from a single-Hole nozzle using a high speed camera. They compared frequency of bubble formation in a rotating bubble bath with stationary one and concluded that before a critical value of cross-flow velocity, ratio of frequencies is unity and after that changes in a complex manner. In another research, Badam et al. [24] perused regimes of bubble formation experimentally utilizing high speed camera. They found that at high gas flow rates, bubble formation frequency remains constant and also bubble volume is almost independent of surface tension. Also, Zhang et al. [25] worked on drag coefficient on bubble rising. In this paper, they calculated the volume of bubble by dividing gas flow rate to bubble formation frequency. They measured frequency of bubble formation by counting the bubbles generated in a time interval. In addition, Hanafizadeh et al. [26–28] in a series of studies investigated the formation, growth and detachment of gas bubbles produced from a submerged needle in water using a high speed camera. They concluded that bubble formation frequency is strongly depended on the contact angle and the surface tension and increases with increasing of gas flow rate.

In current work, a new method for calculating bubble frequency is presented. In this method, an electronic device has been designed and constructed that works based on changes in the intensity of the light beam. Also, the frequency is measured with image processing (IP), numerical, and theoretical methods. Finally, errors of methods will be computed in comparison with the IP method (because this technique has been widely used in the literature) and the most accurate method will be specified.

2. Experimental apparatus

Schematic of the experimental setup of the present work is shown in Fig. 1. The experimental system for this project contains a syringe pump, a square column, standard circular needle with 1.6 mm diameter, a light source, high-speed video camera (1200 fps), and frequency meter device. For photographic observations, the square column made from PMMA with dimensions 100mm × 100mm × 300mm and open to the atmosphere at the top was utilized (Fig. 1-1). The height of the liquid is constant and equal to 60 mm above the needle. The camera records movies with 1200 fps and 336×96 pixels (Fig. 1-4) and sends them to the computer (Fig. 1-6) for image processing. In order to wipe out reflections, one 800 W halogen lamp was placed just in front of the camera (Fig. 1-5). The injection system which is located at the bottom of the column was composed of a needle (Fig. 1-2) as a source of injection joint to an automatically controlled syringe pump (Fig. 1-3). The syringe pump was filled with air and the flow rate range is between 50 to 1200 ml/hr. The frequency meter system contains a 200 mW laser (Fig. 1-9), a phototransistor (Fig. 1-7) and an electronic board (Fig. 1-8) for processing data.

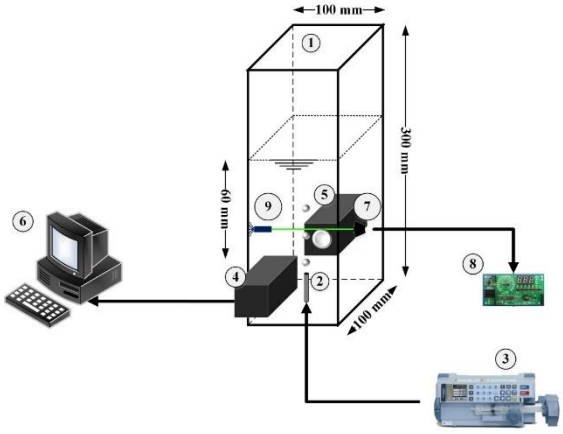

Fig. 1. Schematic view of the experimental setup: (1) bubble column (2) injection needle (3) syringe pump (4) high-speed video camera (5) light source (6) computer (7) phototransistor (8) electronic board (9) laser

The range of operating conditions can be seen in Table 1 (physical properties are computed at 20°C).

Table 1. The range of operating conditions

Operating Parameters	Parameter value
Flow rate	50-1200 mlph
Needle diameter	1.6 mm
Liquid height	60 mm
Liquid viscosity	0.001 Pa. s
Surface tension	72.5×10^{-3} N. m^{-1}
Water Density	997.05 Kg. m^{-3}
Air Density	1.15 Kg. m^{-3}

When the variables are the values of experimental measurements, they have uncertainties due to measurement limitations. For present research, the uncertainties of measured data are shown in Table 2. In this table, based on the accuracy of the measuring instruments, the precision of the major parameters is reported. Moreover, based on analysis of the uncertainty of the Lazar study [29], the uncertainty of the bubble diameter and volume are computed.

Table 2. The uncertainty of the experimentally measured variables.

Parameters	Amount of uncertainty	Percentage of uncertainty
Air flow rate	–	3%
Needle diameter	0.005 mm	–
Physical calibration Scale	0.005 mm	–
Image calibration scale	1 $pixel$	–
Bubble diameter	0.05 mm	–
Bubble volume	0.1 mm^3	–

3. Methodology

As mentioned before, four methods have been utilized in this project in order to measure the frequency of bubble formation: Image processing (IP), frequency device, numerical modeling, and theoretical model. Each of this methods will be explained except IP method. For the detail of the IP method please see the reference [30].

3.1. *Frequency measurement unit*

In order to measure the frequency of bubble formation, continues light beam is embedded just above the needle, which is received by a phototransistor as shown in Fig. 1. When bubbles go through this light beam, make a deviation on that and change the intensity of light. So, the electrical resistance between two bases of phototransistor changes and this variation sensed by an electronic board. According to the number of interruption and duration time, the frequency of bubble formation can be calculated. Fig. 2 shows the continues (Fig. 2a) and interrupted (Fig. 2b) light beam by rising bubble respectively.

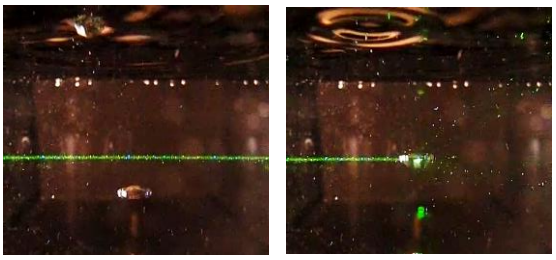

(a) **(b)**

Fig. 2. (a) Continues light beam (b) interrupted light beam by the bubble

The phototransistor is an analog sensor that its electrical resistance changes with the received intensity of light. For measuring this with a microcontroller, the resistance should be converted to voltage in a suitable range. For that reason, a voltage divider is recruited. Voltage divider allows the microcontroller to measure the resistance of the sensor. The sensor is wired in series with a known resistance to form a voltage divider and a known voltage is applied across the divider. Then the center tap of the divider is connected to microcontroller's analog-to-digital converter and the tap's voltage is measured. Then by using the known resistance and voltage, it can compute the resistance of the sensor.

Figure 3 illustrates the measured voltage versus time for different flow rates. The peaks of the charts are related to the moments in which the laser beam is interrupted by rising bubbles. Furthermore, it is clear that with increasing gas flow rate, the distance between peaks gets closer to each other which means the frequency of formation increases. This can be justified by this fact that with increasing gas flow rate, the upward forces acting upon rising bubble dominates downward forces and resulted in a lower time of formation.

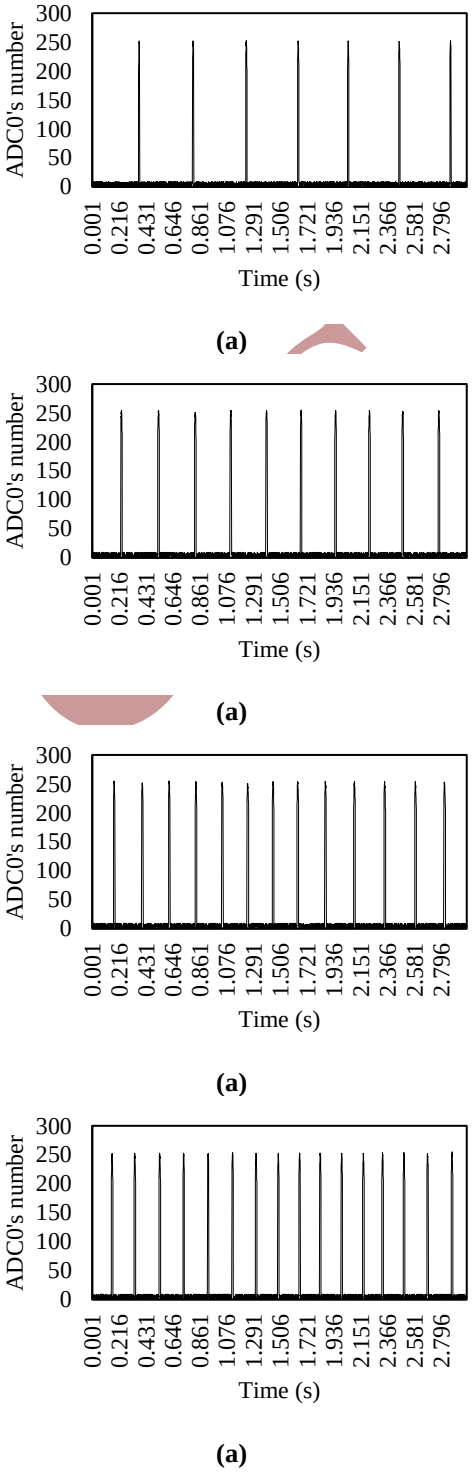

Fig. 3. Fluctuation time for (a) 400 (b) 600 (c) 800 (d) 1000 ml/hr flow rate with frequency device

3.2. *Theoretical Modeling*

For comparison of the obtained results from the presented method, a theoretical model based on force balancing have also used in this paper. Assumptions of force balancing in the theoretical modeling of this study are as the following:

- All properties of fluids are assumed to be constant and are computed at room temperature.
- Bubble growth happens adiabatically and axisymmetric.
- The liquid in the current work is quiescent, so the liquid trust force is not considered.
- The pressure of the gas is uniform within the bubble and the influence of gas viscosity is negligible due to high Reynolds number.
- Gas momentum force is negligible compared with other forces acting on the bubble.
- Because the thickness of the orifice is negligible in comparison with equivalent diameters of that, the contact line between needle and bubble is considered to be fixed to the inner rim of the needle.

Based on the second law of Newton and above assumptions, by considering Fig. 4, the force balance equation can be written as the following:

$$ma = F_B + F_\sigma + F_D + F_V + G \quad (1)$$

where F_B, F_σ, F_D, F_V, and G are buoyancy, surface tension, drag, virtual mass, and gravity forces respectively [31]. So, force balance can be written as follows:

$$m_g a_y = (\rho_l - \rho_g) g V_g - \sigma P sin\theta - \frac{1}{2}\rho_l C_D u_g^2 A - \frac{1}{2} V_g \rho_l a_y \quad (2)$$

By simplifying the above equation, final equation for bubble volume is as follows:

$$V_g = \frac{\rho_l C_D u_g^2 A + 2\sigma P sin\theta}{2(\rho_l - \rho_g)g - (\rho_l + 2\rho_g)a_y} \quad (3)$$

where:
ρ_l: Density of liquid phase
ρ_g: Density of gas phase
C_D: Drag coefficient that is dependent on Reynolds number
u_g: Gas velocity
S: Reference area of the bubble (that is equal to $\pi D^2/4$)
a_y: Acceleration of rising bubble
σ: The surface tension between water and air
θ: Contact angle of the bubble at the detachment
P: Circumference of the injection needle
For Reynolds number between 20 and 260, C_D can be calculated by Ishii formula [32]:

$$C_D = \frac{24}{Re}(1 + 0.1Re^{0.75}) \quad (4)$$

Finally, the frequency of bubble formation can be easily computed by using of flow rate as below:

$$f = \frac{Q}{V_g} = Q \times \frac{2(\rho_l - \rho_g)g - (\rho_l + 2\rho_g)a_y}{\rho_l C_D u_g^2 A + 2\sigma P sin\theta} \quad (5)$$

Where Q is the flow rate of dispersed phase and V_g is the volume of the bubble at the detachment. In this research, velocity and also velocity changes are very small at detachment, so drag force and acceleration are negligible. Therefore, Eqs. (3) and (5) are simplified as below:

$$V_g = \frac{2\sigma P sin\theta}{2(\rho_l - \rho_g)g} \quad (6)$$

$$f = \frac{Q}{V_g} = Q \times \frac{2(\rho_l - \rho_g)g}{2\sigma P sin\theta} \quad (7)$$

Q in the above formula is obtained from syringe pump that plays both roles of injection and controlling flow. ρ_l, ρ_g and σ are physical properties of liquid and gas phase and are measured at 20°C. P is the circumference of the

circular needle that can be easily computed from below equation:

$$P = \pi D \tag{8}$$

where D is the diameter of the needle. Finally, θ is the contact angle of the bubble at detachment that will be computed from experimental data which have been processed with the image processing method. So, a theoretical method is dependent on experimental data due to contact angle.

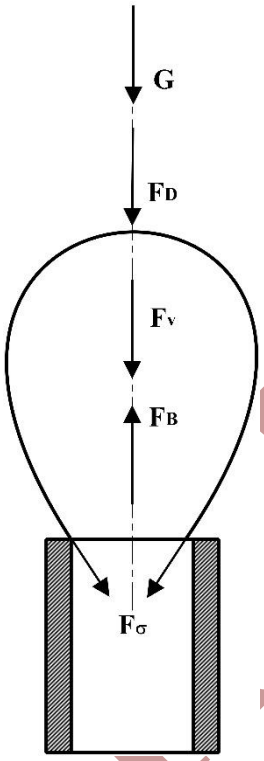

Fig. 4. Schematic of force balance in current project

3.3. *Numerical Modeling*

In this study, the bubble formation process was simulated by applying the VOF method. The flow was supposed to be Newtonian and gas and liquid phases were considered as incompressible fluids. Two or more immiscible fluids can be modeled by the VOF model by solving a single set of momentum equations and exploring the volume fraction of the fluids all over the domain. The VOF formulation based on not osmosing the two or more fluids (or phases). For each additional phase, the volume fraction of the phase in the computational cell is introduced. The volume fractions of all phases sum to unity for each control volume. If the q^{th} fluid's volume fraction in the cell is marked as α_q, then three conditions may be happen [33]:

- $\alpha_q = 0$: The cell is empty (of the q^{th} fluid).
- $\alpha_q = 1$: The cell is full (of the q^{th} fluid).
- $0 < \alpha_q < 1$: The cell contains the interface between the q^{th} fluid and one or more other fluids.

Suitable properties and variables will be determined to each control volume within the domain Based on the local value of α_q.

3.3.1. *Volume fraction equation*

The exploring of the interface(s) between the phases is accomplished by solving the continuity equation for the volume fraction of one (or more) of the phases. For the q^{th} phase, This equation is as follows [33]:

$$\frac{1}{\rho_q}\left[\frac{\partial}{\partial t}(\alpha_q \rho_q) + \nabla \cdot (\alpha_q \rho_q \vec{v}_q) = S_{\alpha_q} + \sum_{p=1}^{n}(\dot{m}_{pq} - \dot{m}_{qp})\right] \tag{9}$$

where $\dot{m}_{pq}$ is the mass transfer from phase q to phase p and $\dot{m}_{pq}$ is the mass transfer from phase p to phase q.
The volume fraction equation will not be solved for the primary phase; the primary-phase volume fraction will be computed based on the following constraint [33]:

$$\sum_{q=1}^{n} \alpha_q = 1 \tag{10}$$

The volume fraction equation can be solved through implicit or explicit time discretization. Because of the faster convergence rate of the explicit method, using this method preferred in this paper.

3.3.2. *The Explicit Scheme*

The formulation of this method can be defined as below [33]:

$$\frac{\alpha_q^{n+1}\rho_q^{n+1} - \alpha_q^n \rho_q^n}{\Delta t} V_c + \sum_f \left(\rho_q U_f^n \alpha_{q,f}^n\right) = \left[S_{\alpha_q} + \sum_{p=1}^{n}\left(\dot{m}_{pq} - \dot{m}_{qp}\right)\right] V \quad (11)$$

where $n+1$: Index for new (current) time step

n: Index for previous time step

$\alpha_{f,q}$: Face value of the q^{th} volume fraction

V_c: Volume of the cell

U_f: Volume flux through the face, based on normal velocity

This formulation does not require the iterative solution of the transport equation during each time step.

3.3.3. *Momentum equation*

Throughout the domain, a single momentum equation is solved and the resulting velocity field is shared between the phases. As below, The momentum equation is dependent on the volume fractions of all phases through the properties ρ and μ [33]. It should be noted that both phases in the present study are considered to be incompressible.

$$\frac{\partial}{\partial t}(\rho\vec{v}) + \nabla.(\rho\vec{v}\vec{v}) = -\nabla p + \nabla.[\mu(\nabla\vec{v} + \nabla\vec{v}^T)] + \rho\vec{g} + \vec{F} \quad (12)$$

In cases with large velocity differences between the phases, the accuracy of the velocities calculated near the interface can be adversely affected and this is one restriction of the shared-field approximation.

In Fig. 5 bubble formation sequence as a comparison between experimental and numerical methods for 800 ml/hr flow rate can be seen. Generally, the formation of bubble happens in three different stages: weeping, expansion, and detachment. In the first stage, the bubble does not conduct due to the high contribution of downward forces. In next stage, a bubble formed with low velocity, so upward and downward forces are approximately equal at this stage. In the final stage, upward forces dominate downward ones and an acceleration movement happens. Also, as shown in this figure, the numerical method can predict the sequence of the bubble formation pretty well and has a good agreement with the real bubble formation process.

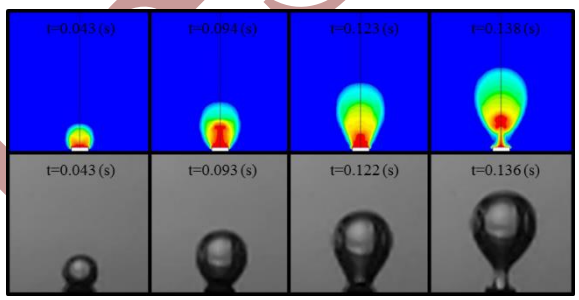

Fig. 5. Comparison of bubble formation sequence between numerical and experimental data for 800 ml/hr flow rate

In order to calculate the bubble frequency formation with numerical method, contours of volume fraction are gathered as picture files and then by image processing method, the frequency is computed.

Results and Discussion

Results are divided into two sections: results of frequency device as the main approach of the current paper, and the results of other methods. In first section details of gathering processing data by frequency, the device is explained and presented. In the next section, results of other methods are just presented.

The results which are gathered by frequency device are shown in Fig. 6. As shown in these diagrams, ADC0's number versus time can be seen. By interrupting the light beam by bubbles, the ADC0's number reaches approximately 250. So by number of peaks in diagrams and duration

time of them, the frequency of bubble formation can be easily computed. Also, it is clear from the figure that with increasing gas flow rate, number of picks in a certain time increases, which means the frequency of formation increases.
The results of methods applied for measuring frequency of formation for different flow rates are shown in Table 3.

Table 2. Comparison of frequency results of different methods

Flow rate (ml/hr)	Image processing (Hz)	Frequency Device (Hz)	Numerical (Hz)	Theoretical (Hz)
50	0.4836	0.4754	0.7097	0.4886
100	1.0093	0.9894	1.4493	0.9491
200	1.8519	1.8186	2.0534	1.7908
400	3.4823	3.4448	3.5714	3.5218
600	5.2131	5.1570	5.6818	5.2570
800	7.0468	6.9655	6.8966	6.9382
1000	8.4906	8.3219	8.8757	8.6539
1200	10.8768	10.6704	10.1371	10.3837

As the image processing technique has been used widely in the literature, the obtained results of the other methods were compared with IP method. The calculated percentage of errors were tabulated in Table 4. The presented errors are computed according to the following formula:

$$\%Error = \frac{f_{IP} - f_i}{f_{IP}} \times 100 \qquad (13)$$

where f_{IP} and f_i are the frequency of bubble formation measured from image processing and other methods respectively.

Table 4. Errors of different methods in comparison with IP method

Flow rate (ml/hr)	Frequency Device (%)	Numerical (%)	Theoretical (%)
50	1.6956	46.7535	1.0339
100	1.9717	43.5946	5.9645
200	1.7982	10.8807	3.2993
400	1.0769	2.5587	1.1343
600	1.0761	8.9908	0.8421
800	1.1537	2.1315	1.5411
1000	1.9869	4.5356	1.9233
1200	1.8976	6.8007	4.5335

As shown in Table 4, generally the results of frequency device have most accordance with IP. It shows that in spite of the low cost of this device, its accuracy is acceptable. Also, errors of theory model show that in the current range of flow rates (50 to 1200 ml/hr) and present operating conditions, balance of forces can be easily defined as a balance of buoyancy and surface tension forces which demonstrate assumptions for deriving equation (7) were admissible. Finally, as shown in the above table, the numerical method has the lowest accuracy especially at high flow rates but is not so far from actual results. One major reason of this low accuracy is the difficulty of modeling the interface of gas and liquid phases in the numerical model due to the numerical diffusion and need to a high grid resolution, which result in a non-sharp interface.
Figure 6 shows the frequency of bubble formation versus flow rate for four mentioned methods. As can be seen, the frequency of formation increases approximately linear with increasing gas flow rate. It can be justified with this fact that increasing gas flow rate tends to the increase in momentum of the bubble and as a result faster detachment of that, which resulted in higher frequency of formation at higher flow rates. As shown in this figure, frequency device

method has the most precision between two other methods (numerical and theory model). Also, results are conforming to previous researches which by increasing flow rate of gas injection, the frequency of bubble formation increases.

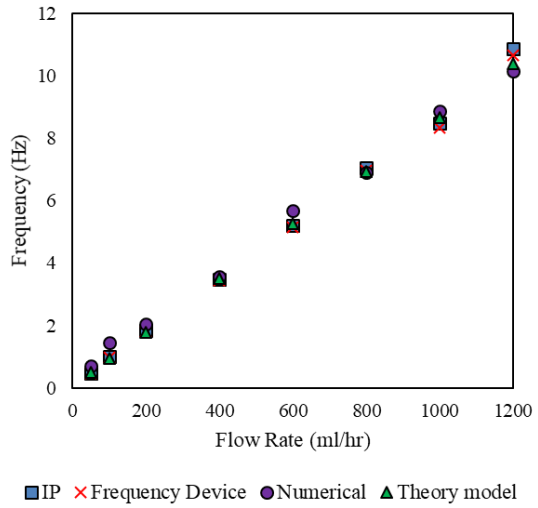

Fig. 6. Frequency of bubble formation versus flow rate for four methods

Also, in Fig. 7 diagram of IP versus frequency device method is illustrated. The average root mean square error between results of frequency device and image processing method is less than 2%. Therefore, this shows that the device has good accuracy.

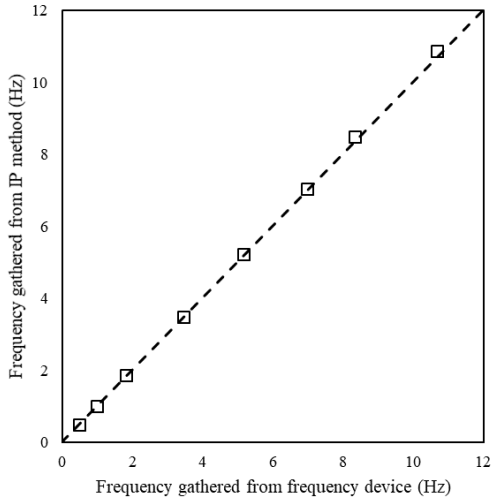

Fig. 7. Frequency of bubble formation from IP method versus frequency device method

To put the accuracy of this method into perspective, two of the most important correlations presented for calculating volume of the bubble at detachment in constant flow condition are taken into account. Then using Eq. (7), frequency of formation for each correlation has been calculated and are compared with the experimental data of the present study in Fig. 8. As can be seen, both correlations presented by Gaddis and Vogelpohl [34] and Jamialahmadi et al. [35] have good agreement with the experimental data specially at relatively low flow rates. The most error between the experimental data and Gaddis and Vogelpohl correlation is about 14%, while this error for Jamialahmadi et al. correlation is about 18%.

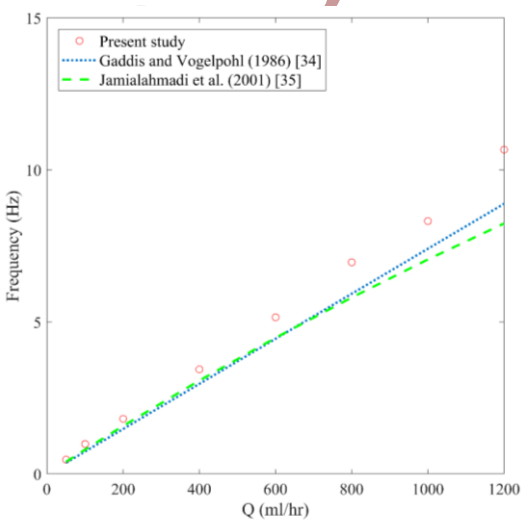

Fig. 8. Prediction of frequency from various correlations and experimental data of present work

Conclusion

In this paper, an electronic device was designed and constructed for measuring the frequency of bubble formation based on a change in intensity of laser beam. Main features of the device are:

- High accuracy despite the low cost
- The ability of momentary measuring of bubble or any other object frequency for industrial applications
- Simple electronic circuit
- So simple to utilizing

The accuracy of this new method was compared with other common methods: IP, numerical and

theoretical modeling. Results showed that this method has very good accuracy. The average root mean square error between results of frequency device and image processing method is less than 2%. So, it can be used as an alternative manner of image processing in many applications.

References

[1] M. G. Reddy, M. V. V. N. L. S. Rani, K. G. Kumar, and B. C. Prasannakumara, "Cattaneo–Christov heat flux and non-uniform heat-source/sink impacts on radiative Oldroyd-B two-phase flow across a cone/wedge," *J. Brazilian Soc. Mech. Sci. Eng.*, vol. 40, no. 2, p. 95, Feb. 2018.

[2] M. G. Reddy and O. D. Makinde, "Magnetohydrodynamic peristaltic transport of Jeffrey nanofluid in an asymmetric channel," *J. Mol. Liq.*, vol. 223, pp. 1242–1248, Nov. 2016.

[3] M. Gnaneswara Reddy and N. Sandeep, "Free convective heat and mass transfer of magnetic bio-convective flow caused by a rotating cone and plate in the presence of nonlinear thermal radiation and cross diffusion," *J. Comput. Appl. Res. Mech. Eng.*, vol. 7, no. 1, pp. 1–21, Aug. 2017.

[4] L. Davidson and J. Erwin H. Amick, "Formation of Gas Bubbles at Submerged Orifices," *AIChE J.*, vol. 5, no. 3, pp. 319–324, 1956.

[5] S. Ramakrishnan, R. Kumar, and N. R. Kuloor, "Studies in bubble formation—I bubble formation under constant flow conditions," *Chem. Eng. Sci.*, vol. 24, no. 4, pp. 731–747, Apr. 1969.

[6] K. Akita and F. Yoshida, "Gas Holdup and Volumetric Mass Transfer Coefficient in Bubble Columns. Effects of Liquid Properties," *Ind. Eng. Chem. Process Des. Dev.*, vol. 12, no. 1, pp. 76–80, Jan. 1973.

[7] E. Sada, A. Yasunzshz, S. Katoh, and M. Nishioka, "Bubble Formation in Flowing Liquid," *Can. J. Chem. Eng.*, vol. 56, no. 6, pp. 669–672, 1978.

[8] H. Tsuge and S.-I. Hibino, "Bubble Formation From an Orifice Submerged in Liquids," *Gordon Breach. Sci. Publ. Inc.*, vol. 22, no. November 2014, pp. 63–79, 1983.

[9] I. Kim, Y. Kamotani, and S. Ostrach, "Modeling bubble and drop formation in flowing liquids in microgravity," *AIChE J.*, vol. 40, no. 1, pp. 19–28, Jan. 1994.

[10] A. . Byakova, S. . Gnyloskurenko, T. Nakamura, and O. . Raychenko, "Influence of wetting conditions on bubble formation at orifice in an inviscid liquid Mechanism of Bubble Evolution," *Colloids Surfaces A Physicochem. Eng. Asp.*, vol. 229, no. 1–3, pp. 19–32, Nov. 2003.

[11] G. Corchero, a. Medina, and F. J. Higuera, "Effect of wetting conditions and flow rate on bubble formation at orifices submerged in water," *Colloids Surfaces A Physicochem. Eng. Asp.*, vol. 290, no. 1–3, pp. 41–49, Nov. 2006.

[12] X. Qu and H. Qiu, "Bubble dynamics under a horizontal micro heater array," *J. Micromechanics Microengineering*, vol. 19, no. 9, p. 095008, Sep. 2009.

[13] M. Ohta, Y. Yoshida, and M. Sussman, "A computational study of the dynamic motion of a bubble rising in Carreau model fluids," *Fluid Dyn. Res.*, vol. 42, no. 2, p. 025501, Apr. 2010.

[14] S. Vafaei, P. Angeli, and D. Wen, "Bubble growth rate from stainless steel substrate and needle nozzles," *Colloids Surfaces A Physicochem. Eng. Asp.*, vol. 384, no. 1–3, pp. 240–247, 2011.

[15] S. Di Bari and A. J. Robinson, "Experimental study of gas injected bubble growth from submerged orifices," *Exp. Therm. Fluid Sci.*, vol. 44, pp. 124–137, 2013.

[16] R. J. Benzing and J. E. Myers, "Low frequency bubble formation at horizontal

circular orifices," *Ind. Eng. Chem.*, vol. 47, no. 10, pp. 2087–2090, 1955.

[17] K. Terasaka and H. Tsuge, "Bubble formation under constant-flow conditions," *Chemical Engineering Science*, vol. 48, no. 19. pp. 3417–3422, 1993.

[18] a. Zaruba, E. Krepper, H. M. Prasser, and B. N. Reddy Vanga, "Experimental study on bubble motion in a rectangular bubble column using high-speed video observations," *Flow Meas. Instrum.*, vol. 16, no. 5, pp. 277–287, 2005.

[19] A. K. Das, P. K. Das, and P. Saha, "Formation of bubbles at submerged orifices - Experimental investigation and theoretical prediction," *Exp. Therm. Fluid Sci.*, vol. 35, no. 4, pp. 618–627, 2011.

[20] N. Hooshyar, J. R. Van Ommen, P. J. Hamersma, S. Sundaresan, and R. F. Mudde, "Dynamics of single rising bubbles in neutrally buoyant liquid-solid suspensions," *Phys. Rev. Lett.*, vol. 110, no. 24, pp. 2–5, 2013.

[21] S. B. Harvey, J. P. Best, and W. K. Soh, "Vapour bubble measurement using image analysis," *Meas. Sci. Technol.*, vol. 7, no. 4, pp. 592–604, Apr. 1996.

[22] J. F. Davidson and B. O. G. Schüler, "Bubble formation at an orifice in a viscous liquid," *Chem. Eng. Res. Des.*, vol. 75, pp. S105–S115, 1997.

[23] M. Iguchi, Y. Terauchi, and S. Yokoya, "Effect of Cross-Flow on the Frequency of Bubble Formation from a Single-Hole Nozzle," *Metall. Mater. Trans. B*, vol. 29, no. December, pp. 1219–1225, 1998.

[24] V. K. Badam, V. Buwa, and F. Durst, "Experimental Investigations of Regimes Under Constant Flow Condition," *Can. J. Chem. Eng.*, vol. 85, no. June, pp. 257–267, 2007.

[25] L. Zhang, C. Yang, and Z. S. Mao, "Unsteady motion of a single bubble in highly viscous liquid and empirical correlation of drag coefficient," *Chem. Eng. Sci.*, vol. 63, no. 8, pp. 2099–2106, 2008.

[26] P. Hanafizadeh, J. Eshraghi, E. Kosari, and W. H. Ahmed, "The Effect of Gas Properties on Bubble Formation, Growth and Detachment," *Part. Sci. Technol.*, vol. 6351, no. November, p. 150407162559008, 2015.

[27] S. E. Hosseini-Doost, A. Sattari, P. Hanafizadeh, and M. Molaei, "A method for bubble volume measurement under constant flow conditions in gas – liquid two-phase flow," *Energy Equip. Syst.*, vol. 6, no. 1, pp. 89–99, 2018.

[28] P. Hanafizadeh, A. Sattari, S. E. Hosseini-Doost, A. G. Nouri, and M. Ashjaee, "Effect of orifice shape on bubble formation mechanism," *Meccanica*, vol. 53, no. 10, pp. 1–23, 2018.

[29] E. Lazar, B. Deblauw, N. Glumac, C. Dutton, G. Elliott, and A. Head, "A Practical Approach to PIV Uncertainty Analysis," in *27th AIAA Aerodynamic Measurement Technology and Ground Testing Conference*, 2010, no. July, pp. 1–22.

[30] P. Hanafizadeh, S. Ghanbarzadeh, and M. H. Saidi, "Visual technique for detection of gas–liquid two-phase flow regime in the airlift pump," *J. Pet. Sci. Eng.*, vol. 75, no. 3–4, pp. 327–335, Jan. 2011.

[31] L. Zhang and M. Shoji, "Aperiodic bubble formation from a submerged orifice," *Chem. Eng. Sci.*, vol. 56, no. 18, pp. 5371–5381, 2001.

[32] M. Ishii and N. Zuber, "Drag coefficient and relative velocity in bubbly, droplet or particulate flows," *AIChE J.*, vol. 25, no. 5, pp. 843–855, Sep. 1979.

[33] *Ansys fluent12.0, Theory Guide*, no. January. ANSYS, Inc, 2009.

[34] E. S. Gaddis and A. Vogelpohl, "Bubble formation in quiescent liquids under

constant flow conditions," *Chem. Eng. Sci.*, vol. 41, no. 1, pp. 97–105, 1986.

[35] M. Jamialahmadi, M. R. Zehtaban, H. Muller-Steinhagen, A. Sarrafi, and J. M. Smith, "Study of bubble formation under constant flow conditions," *Chem. Eng. Res. Des.*, vol. 79, no. 5, pp. 523–532, 2001.